DOI: 10.1002/ejic.200800555

A Novel Route Toward Fabrication of Twofold-Shaped CeO_2 Dendrites

Dongen Zhang,*[a,b] Zhiwei Tong,*[a,b] Shanzhong Li,[a] Xiaobo Zhang,[a] and Ailing Ying[a]

Keywords: Nanotechnology / Crystal growth / Absorption / Cyclic voltammetry

Highly uniform twofold-shaped CeO_2 dendrites were successfully prepared in large quantities by using an approach that involves the thermal decomposition of the precursor. The precursor with an average size of 10 μm was prepared from the reaction of $Ce(NH_4)_2(NO_3)_6$ with $CO(NH_2)_2$ at 160 °C in a water/diethanolamine (DEA) complex solution. The influence of DEA on dendrite formation is discussed. The dendritic pattern of precursor is almost retained in the as-prepared product. The optical absorption spectrum indicates that the CeO_2 dendrites have a direct bandgap of 3.42 eV. The electrochemical characteristic of the CeO_2 dendrites structures have been studied by cyclic voltammetry. It was found that the CeO_2 dendrites can greatly improve the electron-transfer ability.

Introduction

As a typical kind of rare earth oxide, ceria, has been the subject of intense interest because of its unique properties, including its oxygen storage capacity[1] and oxygen ion conductivity.[2,3] Because of these characteristics, ceria has been widely used as a promoter in the three-way catalysts for the elimination of toxic autoexhaust gases,[4–6] as oxygen sensors,[7,8] as solid electrolytes in the solid oxide fuel cells, which utilizes their oxygen storage capacity,[9–11] as absorbents for fluoride ion or arsenic-based compounds, and as substances to filter out ultraviolet rays.[12] Cerium oxide also has a high thermal stability, displays optical behavior, electrical conductivity, and diffusivity. Previous research has proven that nano/microcrystalline CeO_2 has superior properties relative to its bulk counterparts.[13] For example, hierarchically mesostructured ceria exhibits a photovoltaic response, while normal ceria does not show this response.[14] Thus, it is urgent to design functional ceria materials with a certain size and shape by simple morphology-controllable routes. In the past few years, the synthesis of some novel CeO_2 structures, including nanorods,[15–18] nanowires,[19–23] nanotubes,[24,25] nanocubes,[26] microplates,[27] and other morphological structures[28–36] have been reported by chemical scientists. In this paper, twofold-shaped CeO_2 dendrites were successfully fabricated for the first time by thermal treatment of the cerium carbonate hydroxide precursor, which was synthesized by hydrothermal reaction of $Ce(NH_4)_2(NO_3)_6{\cdot}6H_2O$ and $CO(NH_2)_2$ at 160 °C in a water/diethanolamine (DEA) complex solution. The deoxidization–precipitation–decomposition route that uses Ce^{4+} as the cerium source is a novel route toward fabrication of CeO_2 particles; the traditional direct precipitation–decomposition route uses Ce^{3+} as the cerium source. The influence of DEA on dendrite formation is discussed. The optical absorption properties of the CeO_2 dendrites were investigated. We also studied the characteristics of the prepared CeO_2 dendrites. The CeO_2 dendrite modified gold electrode was prepared and used to catalyse the oxidation of methyl orange in solution. The results show that the CeO_2 dendrites exhibit an excellent sensing behavior toward methyl orange, which provides a new application for the CeO_2 dendrites.

[a] Department of Chemical Engineering, Huaihai Institute of Technology,
Lianyungang 222005, People's Republic of China
[b] Japan Science and Technology Agency (JST),
Kawaguchi-shi, Saitama, Japan
E-mail: zdewxm@yahoo.com.cn

Results and Discussion

Figure 1 presents the typical XRD pattern of the as-prepared $Ce(OH)CO_3$ samples. All the peaks could be indexed to the hexagonal phase of cerium carbonate hydroxide (JCPDS Data File #32–0189). The strong and sharp reflection peaks suggest that the as-prepared products are well crystallized. No impurity peaks are observed, which indicate the high purity of the final products.

The TGA curve of the precursor is shown in Figure 2a. There are two weight-loss steps in the temperature ranges 30–280 and 280–345 °C. The first weight loss is mainly attributed to the evaporation of H_2O, whereas the second may be ascribed to the decomposition of the precursor. The weight-loss process ceases at 345 °C, and the stable residue can reasonably be ascribed to CeO_2. According to the TGA data, upon calcination of the obtained precursor at 500 °C in air, the precursor was converted into CeO_2. The XRD pattern of the calcined sample is shown in Figure 2b. All the peaks could be indexed to the cubic phase of ceria with fluorite structure (JCPDS Data File #43–1002). The strong

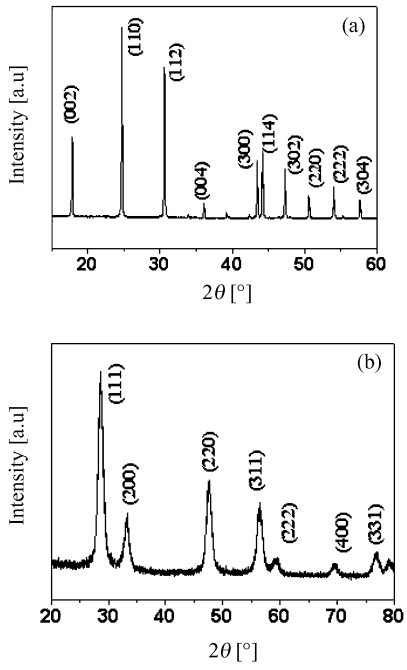

Figure 1. XRD pattern of (a) the $Ce(OH)CO_3$ precursor and (b) the product obtained in the absence of DEA.

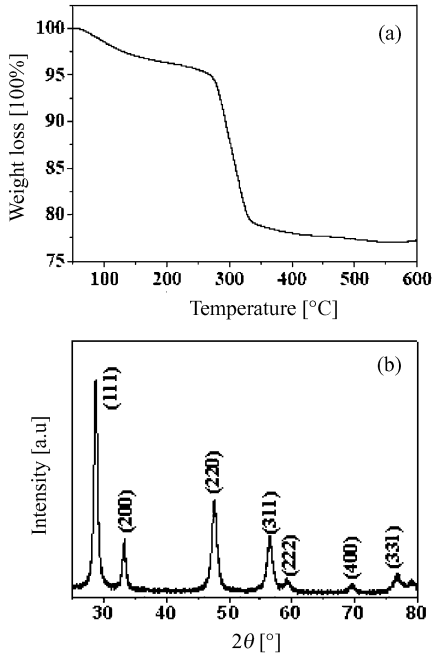

Figure 2. (a) TG curve of the precursor and (b) XRD patterns of the calcined product.

and sharp reflection peaks suggest that the as-prepared products are well crystallized.

The microdendrites were synthesized on a large scale and in high purity. Figure 3 shows typical FESEM images of $Ce(OH)CO_3$ dendrites. The low-magnification image (Figure 3a) shows that the product consists almost entirely of twofold-symmetric structures, and this indicates that high yield and good uniformity is achieved with this approach. The high magnification images (Figure 3b) show that the dendrite was practically made up of two different structural characters, which self-assemble and form a twofold shape. The outer part of each fold is made up of well-aligned arrow-head-like platelets (Figure 3c). While the inner part of each fold is made up of well-aligned grooves that insert into each other at the root of the twofold-symmetric structures (Figure 3d). Close examination of the joint of the twofold shape indicates that the dendrites are actually integrated (Figure 3e) such that sonication for 20 min did not break this nanostructure into discrete particles. The structure and morphology of the dendrites were further examined by TEM and selected-area electron diffraction (SAED). A typical TEM image of a single dendrite is shown in Figure 3f. The SEAD pattern (inset in Figure 3f) of the dendrite suggests that the dendrite is single crystalline.

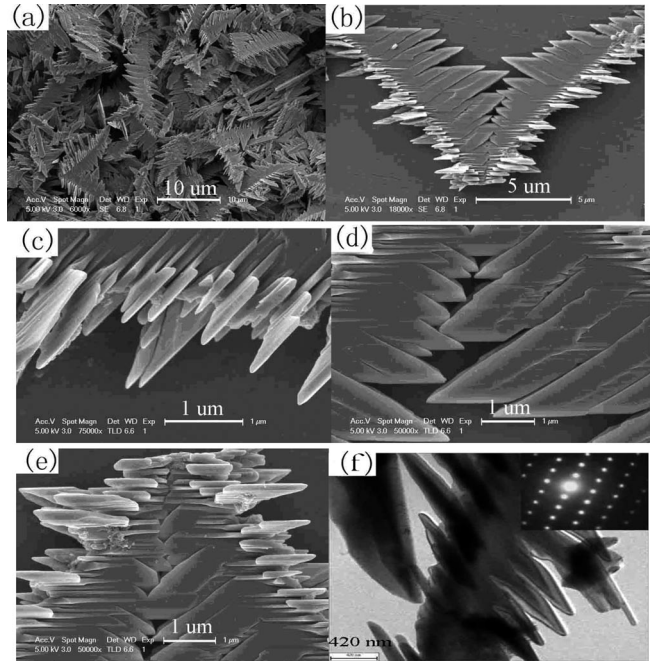

Figure 3. FESEM images of the $Ce(OH)CO_3$ precursor: (a) low magnification, (b) high magnification of one $Ce(OH)CO_3$ dendrite; (c) outer part of the dendrite, (d) inner part of the dendrite, (e) the joint of the twofold dendrite. (f) TEM image of the $Ce(OH)CO_3$ precursor, inset: the corresponding SEAD pattern.

To investigate the nucleation and growth process of the $Ce(OH)CO_3$ dendrites, a series of experiments were carried out for different periods of time. The samples obtained at different reaction times were examined by using FESEM techniques. Figure 4a–d shows the FESEM images of the samples that were fabricated after hydrothermal reaction for 4, 6, 8, and 12 h, respectively. These images clearly reveal the evolution of the $Ce(OH)CO_3$ structures from nanoparticles to dendrites over time at 160 °C. Figure 4a shows that the product mainly consists of nanoparticles. It confirms that $Ce(OH)CO_3$ nanoparticles are formed at first. When the reaction time was increased to 6 h, the nanoparticles started developing into twofold structures (Figure 4b). Further extending the reaction time led to the formation of

uniform dendrites. Figure 4c presents a FETEM image of a sample prepared after heating for 8 h, which shows that the as-obtained products are dominated by dendritic-like structures, and some $Ce(OH)CO_3$ nanoparticles are also observed. When the reaction time was increased to 12 h (as shown in Figure 4d), $Ce(OH)CO_3$ dendrite structures are formed.

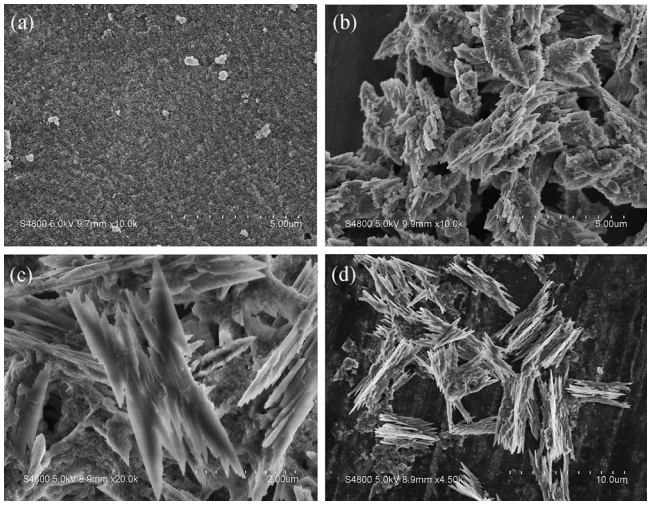

Figure 4. SEM images recorded during the representative growth process of the dendritic structures: (a) 4 h, (b) 6 h, (c) 8 h, and (d) 12 h.

The process for the formation of the $Ce(OH)CO_3$ twofold-symmetric structures may be summarized by the following reactions according to the literature:[37]

$$CO(NH_2)_2 + 3H_2O \rightarrow 2NH_3{\cdot}H_2O + CO_2 \quad (1)$$

$$CO_2 + H_2O \rightarrow CO_3^{2-} + 2H^+ \quad (2)$$

$$Ce^{3+} + NH_3{\cdot}H_2O + CO_3^{2-} \rightarrow Ce(OH)CO_3 + NH_4^+ \quad (3)$$

In the solution synthesis, surfactants or additives are commonly used to regulate the size and shape of inorganic crystals. In the current experiment, the addition of DEA to the reaction mixture obviously influenced the morphology of the obtained $Ce(OH)CO_3$ microcrystals. When the experiments are conducted without DEA, the products are not $Ce(OH)CO_3$ (Figure 1b) and exhibit irregular particle morphology (Figure 5). These results suggest that DEA plays a unique role in the preparation of twofold-shaped $Ce(OH)CO_3$ dendrites. DEA acts as both a reducing and a coordinating agent. A possible reaction process under our experiment conditions may be described as follows: the Ce^{4+} ions are first reduced by DEA to form Ce^{3+} ions because of the high value of the standard electromotive force of the Ce^{4+} ions ($Ce^{4+} + e = Ce^{3+}$, $E^0 = 1.61$ V), and the newly formed Ce^{3+} ions then can coordinate with DEA to form a very stable complex. The two steps sharply decrease the free Ce^{3+} concentration in solution, which slows the rate at which the $Ce(OH)CO_3$ crystals form. It is well known that a slow reaction rate is favorable for crystallization, as well as the separation of the growth and nucleation steps. It is also well known that modification of the reaction steps has great influence on the control of the morphology of nanomaterials.[38] Furthermore, it is generally believed that for a primarily formed crystal with an ultra-small size, agglomeration of the nanoparticles occurs to decrease the exposed surface in order to lower the surface energy.[37] On the basis of the experimental results, the $Ce(OH)CO_3$ microstructures are considered to originate from the assembly and oriented growth of the initially formed $Ce(OH)CO_3$ nuclei. During the agglomeration and growth process, DEA plays multiple roles, not only as the reaction moderator, but also as the structure-directing agent, which determines the direction in which the nuclei grow and aggregate into different structures.[39–41] However, crystallization, electrostatic association within the aggregates, van der Waals forces, hydrophobic interactions, and hydrogen–bonding interactions may also contribute to the formation of the final structure.[42–44] The detailed mechanism for the formation of the final structure by assembling of the primary particles is still a puzzle in nanomaterial research.

After the $Ce(OH)CO_3$ dendrites are calcined in air at 500 °C for 6 h, CeO_2 twofold-symmetric dendrites are formed. As shown in Figure 6, FESEM images reveal that the dendrite shape of $Ce(OH)CO_3$ was sustained after thermal decomposition–oxidation to CeO_2. The edge has an average length of 10 μm. In comparison to $Ce(OH)CO_3$ in Figure 3, the sizes of the CeO_2 dendrites are smaller than that of $Ce(OH)CO_3$ because the density of the former is higher than that of the latter. The SAED pattern (inset in Figure 6f) confirms that the dendrite is crystalline and exhibits discontinuous rings rather than full rings, which indicates that it could consist of CeO_2 polycrystals with an oriented crystallographic axis. The thus-prepared structures

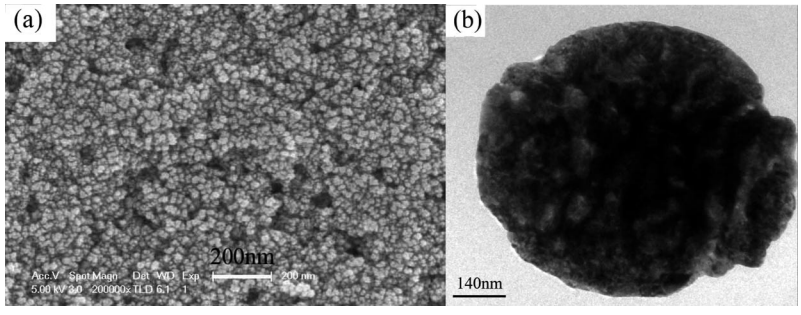

Figure 5. (a) FESEM and (b) TEM images of the product obtained in the absence of DEA.

are very stable, and even ultrasonication over a long period (20 min) could not break them up into discrete platelets, which suggests that the dendrites are integrative.

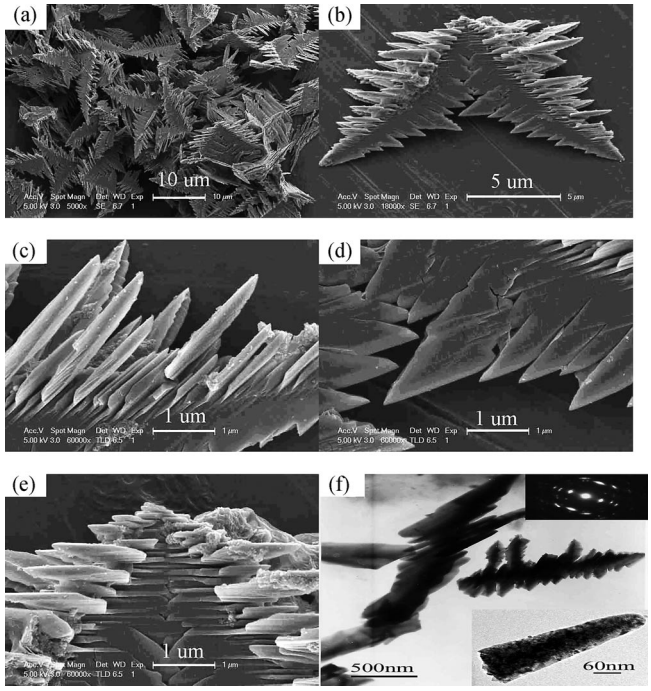

Figure 6. FESEM images of the CeO_2 samples: (a) low magnification, (b) high magnification of one CeO_2 dendrite; (c) outer part of the dendrite, (d) inner part of the dendrite, (e) the joint of the twofold dendrite. (f) TEM image of the CeO_2 samples, inset: the corresponding SEAD pattern.

The UV/Vis absorption spectrum of the CeO_2 sample is shown in Figure 7. It shows that the absorption edge shifts toward shorter wavelengths, i.e. blueshift.[45] The optical bandgap E_g can be determined by the following equation for a semiconductor: $(ah\upsilon)^n = B(h\upsilon - E_g)$,[46,47]where $h\upsilon$ is the photon energy, a is the absorption coefficient, B is a constant relative to the material, and n is either 2 for a direct transition or 1/2 for an indirect transition. The $(ah\upsilon)^2 \approx h\upsilon$ curve for the sample shown in Figure 6b. It reveals that the bandgap of the samples is about 3.42 eV, which is fairly larger than values for bulk powders (3.19 eV) and smaller than that for CeO_2 nanoparticles with an average size of ca. 2.6 nm (4.15 eV). Although the detailed reasons are not clear, size effect may play a part.[48] The selected-area electron diffraction (SEAD) pattern (inset Figure 6f) also confirms that the calcined sample is composed of CeO_2 with a highly polycrystalline structure. It was theoretically deduced that the size of the blueshift, which results from the reduction of the particle size, is inversely proportional to the square of the size because of quantum confinement effects.

Figure 8 exhibits the electrochemical response of methyl orange at the dendrite-modified electrode and the bare gold electrode at 50 mV s^{-1}. Under the same experimental conditions, there was almost no obvious redox peak for methyl

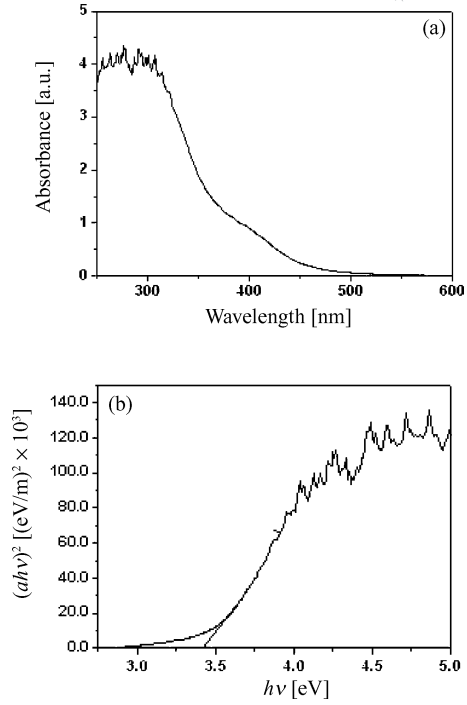

Figure 7. Optical absorption spectrum and $(ah\upsilon)^2 \approx h\upsilon$ curve for the CeO_2 samples.

orange at the bare gold electrode (Figure 8, curve a). However, it can be seen that an oxidation peak potential of methyl orange at dendrite-modified electrode (Figure 8, curve b) appears. Further, the oxidation peak potential for methyl orange at the modified electrode shifts in the negative direction, and the peak current for the same amount of methyl orange increases. It can therefore be concluded that the electrochemical response of methyl orange on the CeO_2 dendrite-modified electrode is better than that on the bare electrode. The above phenomena imply that CeO_2 dendrites can greatly improve the electron-transfer ability, which may be a direct result of the large surface of the dendrite structure. The BET specific surface area of the powders is 4.2 m^2/g, which indicates that the electrochemical probe can arrive at the surface of the electrode more easily. This sug-

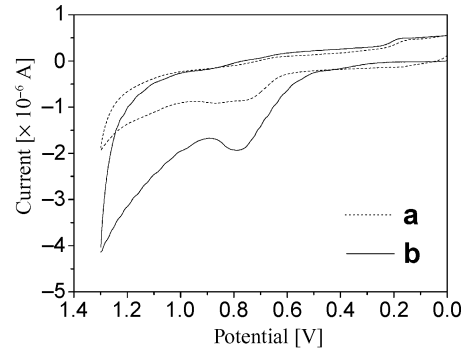

Figure 8. CV performance of 100.0 mg/L methyl orange at different electrodes at a scan rate of 50 mV s^{-1}: (a) bare gold electorde, (b) dendrite-modified GC electrode.

gests that the electrocatalytic activity of the modified electrode could be applied to the electrolysis of the catalytic oxidation of methyl orange.

Conclusions

In summary, we have successfully synthesized twofold-shaped CeO_2 dendrites from a single precursor by thermal decomposition. The precursor was synthesized by hydrothermal reaction by using $Ce(NH_4)_2(NO_3)_6$ and $CO(NH_2)_2$ at 160 °C in a water/DEA solution. Diethanolamine as a multidentate coordination agent play a very important role in the formation of precursor dendrites. The morphology of the precursor was maintained during the heating process. The optical absorption spectrum indicates that the CeO_2 dendrites have a direct bandgap of 3.42 eV. The electrochemical response of the as-prepared dendrite samples with methyl orange was also investigated. The as-prepared CeO_2 dendrites exhibit an excellent sensing behavior toward methyl orange.

Experimental Section

All the analytical chemicals were purchased from the Shanghai Chemical Reagents Company and used without further purification. A typical experiment was as follows: DEA (5 mL) were added to an aqueous solution of $Ce(NH_4)_2(NO_3)_6$ (0.15g, 35 mL of the aqueous solution) whilst stirring. Urea (0.3 g) was then added. The whole mixture was stirred for another 30 min to obtain a homogeneous solution and subsequently transferred into a 50 mL autoclave. The autoclave was maintained at 160 °C for 24 h and then cooled to room temperature by cold water. The white precipitate was then centrifuged, washed with absolute alcohol and distilled water, and dried at 80 °C under vacuum. Finally, to obtain CeO_2, a part of the dry powder was heated to 500 °C for 6 h at a heating rate of 5 °C min^{-1}. X-ray powder diffraction (XRD) patterns were obtained with a Philips X′Pert PRO SUPER X-ray diffractometer equipped with graphite-monochromatized Cu-K_α radiation (λ = 1.5418 Å). Field emission scanning electron microscopy (FESEM) images were taken with a JEOL JSM6700F scanning electron microscope. Optical absorption spectra were recorded on a Shimadzu UV-2401PC UV/Vis recording spectrophotometer.

Acknowledgments

This work was supported by a Grant-in-aid for Scientific Research from the Japan Society for the Promotion of Science (JSPS) and the CREST program of the Japan Science and Technology Agency (JST). We are grateful to the academic leaders of the Jiangsu Province universities' "blue and green–blue project". We are also grateful to the electron microscope and X-ray diffraction facilities group of the University of Science and Technology of China for assistance with the XRD and FESEM measurements.

[1] A. Trovarelli, *Catal. ReV. Sci. Eng.* **1996**, *38*, 439–520.
[2] H. Inaba, H. Tagawa, *Solid State Ionics* **1996**, *83*, 1–16.
[3] L. S. Zhong, J. S. Hu, A. M. Cao, Q. Liu, W. G. Song, L. J. Wan, *Chem. Mater.* **2007**, *19*, 1648–1655.
[4] T. Yuzhakova, V. Rakić, C. Guimon, A. Auroux, *Chem. Mater.* **2007**, *19*, 2970–2981.
[5] M. Lunderg, B. Skaerman, F. Cesar, L. R. Wallenberg, *Microporous Mesoporous Mater.* **2002**, *54*, 97–103.
[6] S. C. Laha, R. Ryoo, *Chem. Commun.* **2003**, *17*, 2138–2139.
[7] H. J. Beie, A. Gnöich, *Sensors Actuators B* **1991**, *4*, 393–399.
[8] P. Jasinski, T. Suzuki, H. U. Anderson, *Sensors Actuators B* **2003**, *95*, 73–77.
[9] B. C. H. Steele, *Solid State Ion.* **2000**, *129*, 95–110.
[10] J. P. Nair, E. Wachtel, I. Lubomirsky, J. Fleig, J. Maier, *Adv. Mater.* **2003**, *15*, 2077–2081.
[11] H. Inaba, H. Tagawa, *Solid State Ion.* **1996**, *83*, 1–16.
[12] R. J. Qi, Y. J. Zhu, G. F. Cheng, Y. H. Huang, *Nanotechnology* **2005**, *16*, 2502–2506.
[13] F. Zhou, X. M. Zhao, H. Xu, C. G. Yuan, *J. Phys. Chem. C* **2007**, *111*, 1651–1657.
[14] S. Carrettin, P. Concepcion, A. Corma, J. M. L. Nieto, V. F. Puntes, *Angew. Chem. Int. Ed.* **2004**, *43*, 2538–2540.
[15] S. C. Kuiry, S. D. Patil, S. Deshpande, S. Seal, *J. Phys. Chem. B* **2005**, *109*, 6936–6939.
[16] H. X. Mai, L. D. Sun, Y. W. Zhang, R. Si, W. Feng, H. P. Zhang, H. C. Liu, *J. Phys. Chem. B* **2005**, *109*, 24380–24385.
[17] K. B. Zhou, X. Wang, X. M. Sun, Q. Peng, Y. D. Li, *J. Catal.* **2005**, *229*, 206–212.
[18] D. E. Zhang, X. M. Ni, H. G. Zheng, X. J. Zhang, J. M. Song, *Solid State Science* **2006**, *8*, 1920–1925.
[19] G. S. Wu, T. Xie, X. Y. Yuan, B. C. Cheng, L. D. Zhang, *Mater. Res. Bull.* **2004**, *39*, 1023–1028.
[20] M. Yada, S. Sakai, T. Torikai, T. Watari, S. Fyruta, H. Katsuki, *AdV. Mater.* **2004**, *16*, 1222–1226.
[21] C. W. Sun, H. Li, Z. X. Wang, L. Q. Chen, X. J. Huang, *Chem. Lett.* **2004**, *133*, 662–663.
[22] R. Yang, L. Guo, *J. Mater. Sci.* **2005**, *40*, 1305–1307.
[23] R. J. La, Z. A. H. L. Hu, Li, X. L. Shang, Y. Y. Yang, *Mater. Sci. Eng. A* **2004**, *368*, 145–148.
[24] W. Q. Han, L. J. Wu, Y. M. Zhu, *J. Am. Chem. Soc.* **2005**, *127*, 12814–12815.
[25] R. Yang, L. Guo, *Chin. J. Inorg. Chem.* **2004**, *20*, 152–158.
[26] S. W. Yang, L. Gao, *J. Am. Chem. Soc.* **2006**, *128*, 9330–9331.
[27] Z. Y. Guo, F. L. Du, Z. L. Cui, *Inorg. Chem.* **2006**, *45*, 4167–4169.
[28] C. W. Sun, J. Sun, G. L. Xiao, H. R. Zhang, X. P. Qiu, H. Li, L. Q. Chen, *J. Phys. Chem. B* **2006**, *110*, 13445–13452.
[29] N. Sakamoto, T. Inoue, K. Kato, *Cryst. Growth Des.* **2003**, *3*, 115–116.
[30] C. Laberty-Robert, J. W. Long, E. M. Lucas, K. A. Pettigrew, R. M. Stroud, *Chem. Mater.* **2006**, *18*, 50–58.
[31] N. Du, H. Zhang, B. Chen, X. Ma, D. Yang, *J. Phys. Chem. C* **2007**, *111*, 12677–12680.
[32] S. Maensiri, C. Masingboon, P. Laokul, W. Jareonboon, V. Promarak, P. L. Anderson, S. Seraphin, *Cryst. Growth Des.* **2007**, *7*, 950–955.
[33] D. E. Zhang, X. J. Zhang, X. M. Ni, J. M. Song, H. G. Zheng, *ChemPhysChem* **2006**, *7*, 2468–2470.
[34] D. E. Zhang, X. J. Zhang, X. M. Ni, J. M. Song, H. G. Zheng, *Chem. Phys. Lett.* **2006**, *430*, 326–330.
[35] W. H. Shen, X. P. Dong, Y. F. Zhu, H. R. Chen, J. L. Shi, *Microporous Mesoporous Mater.* **2005**, *85*, 157–162.
[36] J. Roggenbuck, H. Schäfer, T. Tsoncheva, C. Minchev, J. Hanss, M. Tiemann, *Microporous Mesoporous Mater.* **2007**, *101*, 335–341.
[37] S. F. Wang, F. Gu, C. Z. Li, H. M. Cao, *J. Cry. Grow.* **2007**, *307*, 386–394.
[38] X. M. Ni, Q. B. Zhao, H. G. Zheng, B. B. Li, J. M. Song, D. E. Zhang, X. J. Zhang, *Eur. J. Inorg. Chem.* **2005**, *23*, 4788–4793.
[39] M. Wang, Q. L. Huang, X. T. Chen, X. Z. You, *Mater. Lett.* **2007**, *61*, 4666–4669.
[40] H. N. Wang, Z. Y. Guo, F. L. Du, *Mater. Chem. Phys.* **2006**, *98*, 422–424.
[41] V. Železnỳ, J. Buršík, P. Vaněk, *J. Eur. Ceram. Society,.* **2005**, *25*, 2155–2159.

[42] Y. Politi, T. Arad, E. Klein, S. Weiner, L. Addadi, *Science* **2004**, *306*, 1161–1164.
[43] H. Colfen, M. Antonietti, *Angew. Chem. Int. Ed.* **2005**, *44*, 5576–5591.
[44] H. Colfen, S. Mann, *Angew. Chem. Int. Ed.* **2003**, *42*, 2350–2365.
[45] C. W. Sun, H. Li, H. R. Zhang, Z. X. Wang, L. Q. Chen, *Nanotechnology* **2005**, *16*, 1454–1463.
[46] H. I. Chen, H. Y. Chang, *Ceramics International* **2005**, *31*, 795–802.
[47] J. J. Miao, H. Wang, Y. R. Li, J. M. Zhu, J. J. Zhu, *J. Cryst. Growth* **2005**, *281*, 525–529.
[48] X. H. Liao, J. M. Zhu, J. J. Zhu, J. Z. Xu, H. Y. Chen, *Chem. Commun.* **2001**, *10*, 937–938.

Received: May 31, 2008
Published Online: November 4, 2008

